Fluid dynamic investigation of innovative intake strategies for multivalve internal combustion engines

Alessandra Nigro, Angelo Algieri*, Carmine De Bartolo, Sergio Bova

Department of Mechanical, Energy and Management Engineering (DIMEG) - University of Calabria

Via P. Bucci, Cubo 44C – 87036 Arcavacata di Rende (CS) – Italy

E-mail: anigro@unical.it, a.algieri@unical.it, c.debartolo@unical.it, sergio.bova@unical.it

Abstract

The aim of the paper is to investigate the influence of novel opening strategies for intake valves on the permeability and in-cylinder flow of a multivalve spark-ignition internal combustion engine. Specifically, the deactivation of an intake valve and asymmetric valves lifts are analysed and compared to the standard symmetric valves opening.

To this purpose, a computational fluid dynamic (CFD) analysis is performed by using a finite volume code and an experimental activity is done at a steady flow rig.

The investigation is carried out for different intake strategies and engine load conditions and the comparison between CFD and experimental flow coefficients shows a good agreement.

The results demonstrate that the proper combination of different valves strategies permits the effect of the throttling process at medium and low engine load to be minimised, improving the breathability of the intake system, and creating more organised and energised mean flow structures within the combustion chamber.

Keywords

Internal combustion engines, intake strategies, internal flows, computational fluid dynamics, experimental analysis, engine breathability.

* Corresponding author: a.algieri@unical.it

1. Introduction

The development of more efficient internal combustion engines (ICEs) requires a detailed investigation of the intake phase in order to reduce both fuel consumptions and exhaust emissions and to improve the performances of actual engines [1-5]. To this purpose, special attention should focus on the throttling process and on the intake valves opening. At medium and low engine loads the throttle valve introduces significant pumping losses, decreasing the engine head permeability and increasing fuel consumption [6-8]. For this reason, in the last few years many researchers and automotive manufacturers have been developing innovative intake strategies to guarantee a more efficient process. Variable valve timing (VVT) systems are widely used to reduce the throttle effect. Specifically, early intake valve closure (EIVC), late inlet valve closing (LIVC), and reduced valve lift permit interesting improvements in fuel economy and exhaust emissions at part load [9-12].

Furthermore, in multivalve engines the deactivation of an intake valve is considered a promising strategy to increase efficiency at low engine load [13-16]. As an example, Moore et al. showed the positive effect of valve deactivation on the combustion stability, fuel consumption, and emissions in a 2 litre gasoline direct injection (GDI) engine for loads lower than 6 bar bmep (brake mean effective pressure) [13] and similar results were registered by Patel et al., who analysed a single-cylinder direct injection spark ignition engine [16]. Jovanović et al. focused attention on a 4-valve engine and illustrated that the valve deactivation strategy induced a stronger in-cylinder flow structure near to the top dead centre with the generation of a swirling flow and a proper flow spatial distribution [17]. At the same time, Wilson et al. noticed an improvement in the combustion stability and a decrease in the specific fuel consumption and emissions when asymmetric valve lifts are adopted at part load [18].

The literature demonstrates that engine performances are noticeably influenced by the in-cylinder phenomena and further investigations on multivalve production engines are necessary to guarantee a profound understanding of these promising intake strategies [14,19]. Several research approaches, based on numerical and/or experimental techniques, are available to analyse in detail the fluid

dynamic behaviour of real internal combustion engines [20-22]. Specifically, Computational Fluid Dynamics (CFD) is a widespread technique emerged from the significant increase in the computational power and the availability of parallel codes able to predict the flow field in complex geometries [23-29]. At the same time, the steady flow rig is an extensively employed equipment, owing to the proper characterisation of the real phases and the possibility of analysing production engines and components [30-34]. As an example, Rabault et al. analysed the intake flow in a diesel engine in terms of flow coefficients and PIV measurements adopting a steady flow test bench [35] while Hartmann et al. characterised the flow at the exit of the intake valves and within the combustion chamber of a single-cylinder engine in steady-state conditions adopting a numerical and an experimental approach [36]. According to Pajković and Petrović, in fact, the influence of dynamic effects on the fluid dynamic performances of the intake apparatus of internal combustion engines is negligible, as a consequence, the intake systems are usually characterised in steady-state conditions, at constant ambient-cylinder pressure drop and fixed valve lift [37]. Similar evidences were found by Smith et al., Weclas et al., and Desantes et al. [38-40].

This paper aims to investigate the influence of alternative intake strategies based on the inlet valve deactivation and asymmetric valve lifts on the breathability and in-cylinder flow of a four-stroke multivalve production engine. A comparison with the standard configuration characterised by symmetric valves opening is also performed.

To this purpose SolidWorks Flow Simulation software has been used for the CFD analysis [41]. The code is based on the finite volume discretization and the immersed-boundary method [42-43], a very effective approach to simulate efficiently the flow field within the intake system of a production engine. At the same time, flow coefficients are measured at a steady flow rig to provide global information on engine head breathability and to validate numerical results [44-46].

2. *Experimental apparatus*

The experimental investigation is focused on a production multivalve spark-ignition engine, whose main characteristics are listed in Table 1. The fluid dynamic efficiency of the intake system is analysed at a steady flow rig (Figure 1), enabling air to be forced through the system by means of a blower (A) while the valve lift is fixed to a selected value [47-48]. A by-pass valve (B) permits imposition of the pressure drop between the ambient and the combustion chamber (C). Temperature and pressure transducers (D) are used to characterise the ambient conditions and those inside the cylinder, while a laminar flow meter system (E) is adopted to measure the global mass flow rate.

Engine	**Four-stroke**
Ignition method	Spark-ignition
Compression ratio, r_c	10
Number of cylinders, N_C	2
Number of intake valves per cylinder, N_v	2
Stroke/Bore, L/B	1.068
Intake valve diameter/Bore, D_i/B	0.373
Throttle diameter/Bore, D_t/B	0.745

Table 1: Main engine characteristics.

The engine head is examined in terms of global performances. In particular, the flow coefficients are used to define the head breathability. The global analysis is carried out at several throttle valve positions in order to define the influence of the throttling process on the engine permeability.

Measurements are taken for a fixed ambient-cylinder pressure drop (Δp = 8.3 kPa), while the dimensionless valve lifts (L_v/D_v) are set in the 0.067 ÷ 0.333 interval. In order to investigate the

influence of alternative intake strategies on the fluid dynamic efficiency of the induction apparatus, investigations have been performed for:

i) the standard symmetric valve opening (SV configuration): the same valve lift is imposed for the two intake valves ($L_{v,1} = L_{v,2} = L_v$);

ii) the asymmetric valve opening (AV configuration): the two intake valves are characterised by different lifts ($L_{v,1} \neq L_{v,2}$);

iii) the deactivated valve strategy (DV configuration): only an intake valve is open while the other one is closed ($L_{v,2} = 0$)

where $L_{v,1}$ and $L_{v,2}$ are the lifts of the intake valves 1 and 2 respectively.

The three configurations were examined at wide-open throttle (WOT - F = 90°) condition and at F = 30° in order to evaluate the influence of the throttling process on the engine breathability. Furthermore, the measurements have been repeated also at F = 70° and F = 50° for the traditional symmetric valve opening. Table 2 summarises the analysed configurations and the corresponding measuring conditions.

	Intake valve strategy		
	Symmetric (SV)	Asymmetric (AV)	Deactivated (DV)
Ambient-cylinder pressure drop, Δp	8.3 kPa	8.3 kPa	8.3 kPa
Dimensionless valve lift, L_v/D_v	0.067 ÷ 0.333	0.067 ÷ 0.333	0.067 ÷ 0.333
Dimensionless valve step, $\Delta L_v/D_v$	0.033	0.033	0.033
Throttle angle, F	30, 50, 70, 90°	30, 90°	30, 90°

Table 2: Investigated engine configurations and measuring conditions.

2.1 Flow Coefficients

The flow coefficients are used to define the global fluid dynamic efficiency of the intake system [49-50]. Specifically, the dimensionless coefficients C_f are defined as the ratio of the measured mass flow rate $\dot{m}_{meas}$ to reference value $\dot{m}_r$:

$$C_f = \frac{\dot{m}_{meas}}{\dot{m}_r} \tag{1}$$

If the flow is subsonic, the reference mass flow rate is given by:

$$\dot{m}_r = A_r \frac{p_0}{\sqrt{R \cdot T_0}} \left(\frac{p_C}{p_0} \right)^{\frac{1}{\gamma}} \left\{ \frac{2 \cdot \gamma}{\gamma - 1} \left[1 - \left(\frac{p_C}{p_0} \right)^{\frac{\gamma - 1}{\gamma}} \right] \right\}^{\frac{1}{2}} \tag{2}$$

while, if the flow is choked, the mass flow is formalised as follows:

$$\dot{m}_r = A_r \cdot \frac{p_0}{\sqrt{R \cdot T_0}} \cdot \gamma^{\frac{1}{2}} \left(\frac{2}{\gamma + 1} \right)^{\frac{\gamma + 1}{2 \cdot (\gamma - 1)}} \tag{3}$$

where: p_0 is the intake system pressure;

p_C is the cylinder pressure;

T_0 is the intake system temperature;

R is the specific gas constant;

γ is the specific heat ratio;

A_r is the reference area, equal to the valve outer seat area [50]:

$$A_r = \frac{\pi \cdot D_v^2}{4} \tag{4}$$

The overall uncertainty of dimensionless flow coefficients, evaluated according to the literature [51-52], is always lower than 2.1%, and it decreases as valve lift and throttle angle increase.

3. Geometrical model and examined configurations

The CFD simulations are carried out for the 3D geometry shown in Figure 2. This is a complex geometry, mainly made up of the intercooler exit duct and the throttle valve (A), the intake manifold (B), and the engine head with the intake valves and cylinders (C).

Simulations were performed for the different intake strategies defined previously. Specifically, for symmetric valve opening two different positions of the throttle valve (F = 90° and F = 30°) were used, whereas the asymmetric and deactivated configurations were examined in wide-open throttle configuration (Table 3).

To analyse the flow within the combustion chamber three planes perpendicular to the cylinder axis (T1, T2 and T3) and three vertical planes (L1, L2 and L3) were considered, as visible in Figure 3.

Valves configurations	Dimensionless "Valve 1" lift $L_{v,1}/D_v$ [-]	Dimensionless "Valve 2" lift $L_{v,2}/D_v$ [-]	Throttle angle F [°]
Symmetric valves (SV-F90)	0.333	0.333	90
	0.200	0.200	90
	0.067	0.067	90
Symmetric valves (SV-F30)	0.333	0.333	30
	0.200	0.200	30
Asymmetric valves (AV-F90)	0.333	0.200	90
	0.333	0.067	90
	0.200	0.067	90
Deactivated valve (DV-F90)	0.333	0.000	90
	0.200	0.000	90

Table 3: Analysed configurations with CFD.

4. Discretisation and boundary conditions

An immersed boundary (IB) approach for a cell-centred finite volume solver [41] was adopted to compute the turbulent flow field in the engine using Cartesian grids. The IB method [53-55] is based on a special treatment of the boundary conditions that simplifies the grid generation process by allowing the use of structured grids even in complex geometries. Consequently, the time required for mesh generation and successive refinements is greatly reduced with respect to the body-fitted approach. Figure 4a shows a section of the mesh near the intake valve, while Figure 4b depicts the three-dimensional structured hexahedral grid of the engine head.

The governing equations are discretised in a conservative form. The Favre averaged Navier-Stokes equations were used and the turbulence was solved by employing the low Reynolds number form of the k-ε model proposed by Lam-Bremhorst [56]. This approach extends the validity of the Jones and Launder model [57] through the viscous sub-layer to the wall, additionally modifying the turbulent transport equations and the turbulent viscosity by means of the so called low-Reynolds-number (dumping) functions. The near wall treatment is based on the Two-Scale Wall Functions (2SWF) model [58], which is designed to predict laminar, turbulent and transitional boundary layers.

The upwind approximation of the inviscid fluxes is second-order accurate and based on an implicitly treated modified Leonard's QUICK approximation [59] and on the Total Variation Diminishing (TVD) method [60-61] to preserve local monotonicity of the solution.

Time implicit first-order accurate approximations of the momentum, energy and k-ε equations are used together with an elliptic type discrete pressure equation, derived by algebraic transformations of the discrete mass and momentum equations (SIMPLE-like approach), to advance the solution in time efficiently. The linear system of equations is solved using a preconditioned generalised conjugate gradient method [62] with ILU preconditioning. To solve the algebraic system arising from the discrete pressure-correction equations, an iterative procedure based on a multigrid method developed by Hackbusch [63] is used.

Table 4 provides some information about the fine mesh used to discretise the computational domain and the related computational cost in terms of CPU. Grid independence has been ensured by successive solution-adaptive mesh refinements. The convergence was checked by monitoring the variations in the mass flow rate between the inlet and the outlet sections of the computational domain as a function of the iterations. The calculations process was stopped when a very low percentage variation between inlet and outlet mass flow rate was reached ($<10^{-6}$). All the simulations were performed in parallel using 8 computing cores (Intel Xeon E5620 with a clock of 2.40 GHz).

Total cells	~ 6,000,000
Fluid cells	~ 3,500,000
Interface cells	~ 2,500,000
Iterations	~ 700
CPU time	~ 155,000 s

Table 4: Grid resolution and computational resources.

	Fluid dynamic parameters	Turbulence parameters
Inflow:	Total pressure: 99,800 Pa	Intensity: 2.00 %
	Temperature: 295.85 K	Length: 0.005 m
Outflow:	Static pressure: 91,464 Pa	-
	Temperature: 295.85 K	
Wall:	Heat flow = 0 (adiabatic wall)	-
	Velocity = 0 (no-slip condition)	

Table 5: Boundary conditions.

Table 5 summarises the adopted boundary values. The inflow section of the computational domain corresponds to the exit of the intercooler and the outflow to the cylinder exit. Specifically, the

cylinder length was fictitiously extended to 20 times the engine bore in order to enable constant pressure conditions at the exit section to be fixed. Experimental pressures and temperatures were used at inlet and outlet sections. Moreover, the velocity components on the wall were set to zero (non-slip condition).

5. Results

5.1 Experimental analysis

Dimensionless flow coefficients were used to characterise the global fluid dynamic efficiency of the four-valve spark-ignition engine and to validate numerical results. Specifically, the investigation was performed first for the standard (SV) configuration at different throttle angles in order to evaluate the influence of the throttling process on the intake system permeability.

Figure 5 shows the experimental flow coefficients as a function of the dimensionless valve lift (L_v/D_v). The results demonstrate the presence of different flow regimes, characterised by decreasing slopes in the flow coefficient curve, according to the literature [49,64]. Particularly, at low valve lift, the flow remains attached to the valve seat and head due to the high viscous phenomena. A flow separation occurs, first, at the valve head and, successively, at the valve seat when the lift increases. The analysis evidences that the "transition" from one flow condition to another is reached at lower valve lift values when the flow is throttled. In fact, for the wide-open throttle configuration (F = 90°), the transition phenomena take place at $L_v/D_v \sim 0.16$ and $L_v/D_v \sim 0.23$, while for F = 30° they occur at $L_v/D_v \sim 0.12$ and $L_v/D_v \sim 0.16$, respectively.

As expected, a continuous rise in the head permeability is observed when the throttle angle increases, owing to the progressive upsurge in the mass flow rate entering the combustion chamber. However, this effect tends to reduce significantly with the throttle angle and there are negligible effects on the fluid dynamic effectiveness of the intake system when $F \geq 70°$. In this case, the percentage differences with the wide-open throttle configuration are always lower than 3.2% and become lower than 1.2% when the dimensionless valve lift is larger than 0.13. The maximum flow

coefficient is 0.38 and similar values are found for dimensionless lifts larger than 0.27 when the dimensions of the intake ports and valve stems define the minimum flow area. A percentage decrease in head permeability lower than 15% is found moving from F = 70° to F = 50°.

Conversely, a noticeable decrease in the dimensionless parameter and, as a consequence, on the engine fluid dynamic efficiency is registered when the throttle angle is lower than 50° with a reduction that is always higher than 30% moving from F = 50° to F = 30°.

In order to reduce the effect of the throttling process on the engine head breathability and to improve the mean flow structures within the combustion chamber, new intake strategies were investigated. Specifically, the asymmetric (AV) configuration - characterised by different valves lifts for the two intake valves - and the deactivated valve (DV) strategy - with only an intake valve open - were analysed and compared to the standard symmetric valve (SV) configuration (Table 3). Figure 6a and 6b show the deactivated and asymmetric strategy, respectively.

Experimental results confirm the presence of different flow regimes and highlight the large influence of the throttling process on the engine permeability.

For the deactivated (DV) configuration (Figure 6a), the decrease in the flow coefficient is always higher than 24% moving from the wide-open throttle configuration to F = 30° and the difference reaches 42% when the dimensionless valve lift is larger than 0.23. The comparison with the standard configuration at the same throttle angle shows the noticeable reduction in the flow coefficients when an intake valve is closed. Specifically, the mean percentage decrease in the mass flow rate entering the combustion chamber is equal to 49.8% when F = 90° and it is about 28% when the flow is throttled (F = 30°).

Furthermore, the analysis reveals that the proposed deactivated strategy in the wide-open throttle configuration guarantees similar flow coefficients and mass flow rates of the standard intake valves when F = 30°. The result suggests to adopt the unthrottled deactivated strategy to control the engine power at low load, owing to the possibility to guarantee the same mass flow rate entering the cylinder with a lower curtain area and to obtain higher flow coefficients when the same curtain area

is used. This is due to the lower pressure losses at the throttle valve, the better filling of the combustion chamber, and the improved fluid dynamic efficiency of the wide-open throttle configuration.

Figure 6b illustrates the flow coefficients of the asymmetric (AV) configuration as a function of the throttle angle and dimensionless valve lift. As already observed, the higher the throttle angle, the higher the mass flow rate and, consequently, the engine permeability. The comparison with the standard control strategy shows that the asymmetric configuration permits to reproduce all the operating ranges of the standard configuration. It further enables a larger flexibility in the operating conditions and engine control, due to the possibility to impose different lifts between the two intake valves. As an example, when F = 90° the flow coefficient in the standard configuration is equal to 0.30 at $L_v/D_v = 0.167$ while the corresponding dimensionless parameter (at $L_{v,1}/D_v = 0.167$) ranges between 0.22 ($L_{v,2}/D_v = 0.067$) and 0.35 ($L_{v,2}/D_v = 0.333$) when the asymmetric valve opening is adopted.

The experimental analysis highlights that the proper combination of the deactivation (DV) and asymmetric (AV) strategies gives a larger flexibility in the mass flow control, with the possibility of reproducing all the operating range of the standard configuration. Specifically, the deactivation of an intake valve is suggested at low engine load, whereas the asymmetric valves configuration is useful for medium-high mass flow rates. The advantage is the opportunity to create a different and more organised in-cylinder charge motion, as it will be shown in the next section.

5.2 Numerical analysis

To investigate in more detail the flow field within the combustion chamber and to evaluate the influence of the different intake strategies on the fluid dynamic behaviour of the engine, a 3D numerical analysis was performed. Figure 7 illustrates the comparison of experimental and numerical flow coefficients. The analysis highlights that the numerical model characterises the global fluid dynamic efficiency of the engine head with a good accuracy for both standard (SV) and

innovative (AV and DV) configurations, with a mean percentage difference with respect to the experimental measurements of 4.6%. The maximum value (9.3%) has been registered for the symmetric valve opening with throttled flow (F = 30°). This value stems from the corresponding low flow coefficient (0.15) even though the absolute difference between numerical and experimental data is equal to 0.014. It is worthy to notice that for all the investigated configurations the absolute differences are at least one order of magnitude lower than the corresponding experimental results.

5.2.1 Flow field analysis

The assessment of the numerical model permitted the influence of the throttle valve and the effect of the proposed strategies on the intake phase behaviour to be analysed in more detail.

Figure 8 shows the pressure distribution within the intake system for the standard (SV) configuration with 30° (Figure 8a) and 90° (Figure 8b) throttle valve opening. The comparison was carried out at the same pressure difference between ambient and cylinder (Δp = 8.3 kPa), according to the experimental analysis.

It can be noticed that under the part load condition, the pressure drop mainly occurs at the throttle valve (Δp_t = 6.61 kPa) and two different pressure fields are produced upstream and downstream. Conversely, at full load the influence of the throttle is negligible (Δp_t = 0.75 kPa) and the pressure drop is distributed along the intake system.

In order to evaluate the influence of the innovative intake strategies on the in-cylinder flow field, numerical results of deactivated (DV) and asymmetric (AV) valves opening configurations were compared with the standard symmetric (SV) approach at partial and high load condition, respectively.

5.2.2 Part load conditions

The previous global analysis demonstrated that similar mass flow rates are reachable at part load by using the standard (SV) throttled configuration or the deactivated (DV) strategy in WOT configuration. Moreover, the adoption of the alternative approach offers the possibility to significantly reduce the pressure losses at the throttle valve, to modify the in-cylinder flow field, and to improve the global engine efficiency. To this purpose, symmetric (SV) and deactivated (DV) valves opening configurations were compared at similar mass flow rates adopting a 3D numerical analysis. Specifically, the standard configuration refers to a throttle angle of 30° (SV-F30) with valve lifts (L_v/D_v = 0.333) while the deactivated configuration is characterised by wide-open throttle (DV-F90) with only one intake valve open ($L_{v,1}/D_v$ = 0.200).

Figure 9 shows the three-dimensional flow structure inside the cylinder in terms of the velocity-coloured flow trajectories for the two above configurations. The comparison of the two plots allows one to appreciate that the DV-F90 configuration significantly increases the velocities of the flow entering the cylinder and the rotational charge motion within the combustion chamber. Specifically, for the deactivated strategy the velocity near the intake valve is larger than 80 m/s while the corresponding value is always lower than 40 m/s for the standard configuration.

To compare the two configurations in more detail, Figure 10 illustrates the flow field on the three planes orthogonal to the cylinder axis. The streamtrace distributions point out the asymmetric flow pattern and the higher intensity of the tangential velocity component of the DV-F90 configuration with respect to SV-F30 at the plane T1. Furthermore, for DV-F90 the interaction between the inflow and the cylinder walls creates a main swirl motion that becomes more significant moving away from the engine head (from plane T1 to T3). Conversely, in the SV-F30 configuration several smaller vortices are present for this configuration. A symmetric flow pattern is observed on the T1 plane, whereas the vortices coalescence produces more irregular streamtrace distributions on the T2 and T3 planes.

Figure 11 depicts the flow field in vertical planes in terms of velocity contours. The plots in the L1 plane (Figures 11a and 11b) show that the interaction between the inflow and the cylinder wall is

more significant and creates a wide recirculating region behind the intake valve for the deactivated strategy, while an almost symmetric flow pattern with a weak valve to valve flow interaction is observed for the standard valves opening. As expected, striking differences between DV-F90 and SV-F30 contour plots are evident in the L2 plane owing to the valve deactivation (Figures 11c and 11d). Flow similarities are seen in the L3 plane (Figures 11e and 11f). Nevertheless, the expanding annular jet hits the wall and flow along it with higher intensity for DV-F90 compared to SV-F30, with a positive effect on the turbulence kinetic energy and combustion process [17].

5.2.3 High load conditions

The comparison of different intake strategies was extended to high load conditions. Specifically, CFD results of symmetric (SV) and asymmetric (AV) valves opening configurations were investigated. The SV configuration is defined by $L_v/D_v = 0.333$, while AV configuration considers different intake valves lifts ($L_{v,1}/D_v = 0.333$ and $L_{v,2}/D_v = 0.200$). In both cases the throttle valve is wide-open (F = 90°).

Figure 12 shows the velocity-coloured flow trajectories within the cylinder. The comparison of the two plots highlights that the asymmetric configuration creates a higher rotational motion within the combustion chamber.

For both engine conditions, the streamtraces of Figure 13 show a flow structure consisting of vortices of different sizes. In particular, for AV-F90 the tangential velocity induces a more irregular flow pattern with more coherent swirl-type structures than those computed for SV-F90.

Figure 14 shows the velocity contours in the vertical planes. The difference between the plots is strongly reduced compared to Fig. 11 for part load conditions due to the reduced flow unbalancing between the intake valves. Noticeable valve-to-valve and valve-to-wall flow interactions are detected on the L1 plane (Figures 14a and 14b).

Specifically, the highest interference phenomena between the two valves are observed for the symmetric opening. Similar velocity contours are found on the L2 plane as the two configurations

have the same valve lift (Figures 14c and 14d). On the other hand, AV-F90 has a smaller valve lift in the L3 plane that produces a different annular flow expansion, with a well-defined wall jet structure along the cylinder surface (Figures 14e and 14f).

5.2.4 Swirl number

Finally, computational results were used to quantify the flow rotation inside the combustion chamber with respect to the cylinder axis. To this purpose, the angular momentum produced by the tangential velocity (u_{tg}) was combined with the axial mass flow as [65-66]:

$$S = \frac{1}{R} \frac{\int_0^R \int_0^{2\pi} \rho u_{ax} u_{tg} r^2 \, d\vartheta \, dr}{\int_0^R \int_0^{2\pi} \rho u_{ax}^2 r \, d\vartheta \, dr} \tag{5}$$

where S is the swirl number, R the radius of the cylinder, u_{ax} the axial velocity, u_{tg} the tangential velocity, r the radial distance, and ρ is the air density. The swirl numbers reported in Figure 15 and summarised in Table 6 were evaluated on the three transversal planes T1, T2, and T3 (z/B = 0.25, 0.50, and 0.75 respectively, where z is the distance of the plane from the head and B is the engine bore) for the different load conditions according to equation 5. The trends of the absolute values of the swirl number are consistent with the flow patterns of Figures 10 and 13. It can be observed from Table 6 that in DV-F90 configuration the swirl number is negative (clockwise) and increases (in absolute value) with the distance from the engine head, where the flow is more organised owing to the progressive decay of the recirculating structure below the intake valves, as already observed in Figure 10. For the other configurations the swirl number is positive (counterclockwise) and reduces moving away the engine head. Furthermore, Figure 14 shows a higher swirl number for AV-F90 with respect to SV-F30 and SV-F90. In particular, for all the transversal planes the difference in swirl number of the symmetric configurations (F = 30° and F = 90°) is negligible. Thus, it can be concluded that the rotational motion around the cylinder axis is amplified adopting asymmetric and deactivated configurations, owing to the flow unbalancing between the intake valves, while the

rotational intensity is low and independent of the load conditions when the symmetric valves configuration is adopted.

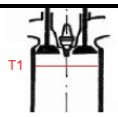
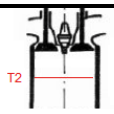
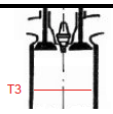
	 Plane T1 (z/B=0.25)	 Plane T2 (z/B=0.50)	 Plane T3 (z/B=0.75)
SV-F90	0.224	0.122	0.048
SV-F30	0.231	0.109	0.063
AV-F90	0.328	0.212	0.163
DV-F90	- 0.163	-0.396	-0.525

Table 6: Swirl number on the three transversal planes for different valves configurations.

6. Conclusions

The work has analysed the fluid dynamic behaviour of an internal combustion engine. In particular, attention has been focused on a production multivalve spark-ignition engine during the intake phase. To this purpose, a numerical and an experimental investigation were carried out to evaluate the influence of novel intake valves opening strategies on the system permeability and on the in-cylinder flow field, highlighting their effectiveness and their advantages with respect to the standard (symmetric) valves opening configurations.

As concerns the numerical analysis, an immersed boundary approach for a cell-centred finite volume solver was adopted to simulate efficiently the flow field using Cartesian grids. For the experimental investigation, the fluid dynamic efficiency of the intake system was analysed at a steady flow rig in terms of flow coefficients. The comparison of numerical and experimental data displayed a good agreement. Specifically, the mean percentage difference between measured and

numerical flow coefficients was equal to 4.6% despite the very complex three-dimensional flow and the large size geometry.

The global investigation has revealed the significant influence of the inlet valve opening on the fluid dynamic efficiency of the intake apparatus. Different flow regimes were observed and flow separation phenomena at the valve head and seat were noticed at medium and high valve lifts. Furthermore, the effect of the throttling process on the engine breathability has been studied. To reduce the throttle losses, it is suggested to deactivate an intake valve at low engine load (deactivation strategy) whereas different lifts between the two intake valves (asymmetric strategy) are proposed at medium-high loads. At low engine load, the deactivated configuration guarantees the same flow coefficients as the standard approach with a lower curtain area and a better engine permeability when the curtain area is fixed. Furthermore, the asymmetric valves configuration reproduces similar mass flow rates to the traditional valves opening with different flow distribution between the two valves.

The characterisation of the flow field within the combustion chamber showed an almost symmetric flow pattern for the standard valves opening configuration with a weak valve-to-valve flow interaction at low engine load that progressively increases with the valve lift. On the other hand, the adoption of the proposed alternative strategies produces a flow unbalancing between the intake valves and an asymmetric flow distribution. As a consequence, the proper combination of the different intake strategies assures a larger flow control and a higher fluid dynamic efficiency (breathability) at all the operating conditions, with the possibility of creating alternative organised in-cylinder flow structures. Specifically, the proposed strategies produce a higher rotational motion and a more organised and energised flow, especially at low engine loads, which could enhance the consequent combustion process. This phenomenon will be investigated in a future work adopting the numerical model validated in this paper.

Acknowledgements

The research has been developed within the framework of the project "Powertrain - PON01_01517, CUP: B21H11000400005", funded by the Italian Ministry of University and Research (MIUR) with the financial support of the European Commission. The authors would like to thank Fakhry Abuzahra, Luigi De Napoli, and Francesco Spadafora for their collaboration.

References

1. R. Barzegar, S. Shafee, S. Khalilarya, CFD simulation of the combustion process, emission formation and the flow field in an in-direct injection diesel engine, Thermal Science, 17 (2013), 11-23.
2. J. M. Desantes, J. Galindo, C. Guardiola, V. Dolz, Air mass flow estimation in turbocharged diesel engines from in-cylinder pressure measurement, Experimental Thermal and Fluid Science, 34 (2010), 37-47.
3. Y. T. Anbese, A. R. A. Aziz, M. R. Heikal, Characteristics of Induction Flow in SI Direct Injection Engine with Dual Variable Swirl Control Valve, Journal of Applied Sciences, 12 (2012), 2534-2540.
4. M. Inagaki, M. Nagaoka, N. Horinouchi, K. Suga, Large eddy simulation analysis of engine steady intake flows using a mixed-time-scale subgrid-scale model, International Journal of Engine Research, 11 (2010), 229-241.
5. Z. S. Jovanović, Z. M. Živanović, Ž. B. Šakota, M. V. Tomić, V. S. Petrović, The effect of bowl-in-piston geometry layout on fluid flow pattern, Thermal Science, 2011, 15: 817-832.
6. G. Fontana, E. Galloni, Variable valve timing for fuel economy improvement in a small spark-ignition engine, Applied Energy, 86 (2009), 96-105.
7. M. Jankovic, S. W. Magner, Cylinder air-charge estimation for advanced intake valve operation in variable cam timing engines, JSAE Review, 22 (2001), 445-452.

8. S. Verhelst, P. Maesschalck, N. Rombaut, R. Sierens, Efficiency comparison between hydrogen and gasoline, on a bi-fuel hydrogen/gasoline engine, International Journal of Hydrogen Energy, 34 (2009), 2504-2510.
9. S. M. Begg, M. P. Hindle, T. Cowell, M. R. Heikal, Low intake valve lift in a port fuel-injected engine, Energy, 34 (2009), 2042–2050.
10. J. Benajes, S. Molina, J. Martín, R. Novella, Effect of advancing the closing angle of the intake valves on diffusion-controlled combustion in a HD diesel engine, Applied Thermal Engineering, 29 (2009), 1947-1954.
11. H. Hong, G. B. Parvate-Patil, B. Gordon, Review and analysis of variable valve timing strategies - eight ways to approach, Proceedings of the Institution of Mechanical Engineers, Part D: Journal of Automobile Engineering, 218 (2004), 1179-1200.
12. T. Leroy, J. Chauvin, N. Petit, Motion planning for experimental air path control of a variable-valve-timing spark ignition engine, Control Engineering Practice, 17 (2009), 1432-1439.
13. W. Moore, M. Foster, M.-C. Lai, X.-B. Xie, Y. Zheng, A. Matsumoto, Charge Motion Benefits of Valve Deactivation to Reduce Fuel Consumption and Emissions in a GDi, VVA Engine, SAE Technical paper 2011-01-1221, 2011.
14. D. Coltman, J. W. G. Turner, R. Curtis, D. Blake, B. Holland, R. J. Pearson, A. Arden, H. Nuglisch, Project Sabre: A Close-Spaced Direct Injection 3-Cylinder Engine with Synergistic Technologies to achieve Low CO2 Output, SAE Technical paper 2008-01-0138, 2008.
15. M. Sellnau, T. Kunz, J. Sinnamon, J. Burkhard, 2-step Variable Valve Actuation: System Optimization and Integration on an SI Engine, SAE Technical paper 2006-01-0040, 2006.
16. R. Patel, N. Ladommatos, P. A. Stansfield, G. Wigley, C. P. Garner, G. Pitcher, J. W. G. Turner, H. Nuglisch, J. Helie, Un-throttling a direct injection gasoline homogeneous mixture

engine with variable valve actuation, International Journal of Engine Research, 11 (2010), 391-411.

17. Z. S. Jovanović, B. S. Basara, M. V. Tomić, V. S. Petrović, Some subtleties concerning fluid flow and turbulence modeling in 4-valve engines, Thermal Science, 15 (2011), 1065-1079.
18. N. D. Wilson, A. J. Watkins, C. Dopson, Asymmetric Valve Strategies and their Effect on Combustion, SAE Paper 930821, 1993.
19. A. Algieri, Fluid Dynamic Efficiency of a High Performance Multi-Valve Internal Combustion Engine During the Intake Phase, Thermal Science, 17 (2013), 25-34.
20. M. A. Jemni, G. Kantchev, M. S. Abid, Influence of intake manifold design on in-cylinder flow and engine performances in a bus diesel engine converted to LPG gas fuelled, using CFD analyses and experimental investigations, Energy, 36 (2011), 2701-2715.
21. S. Ramanathan, A. Hudson, J. Styron, B. Baldwin, D. Ives, D. Ducu, EGR and Swirl Distribution Analysis Using Coupled 1D-3D CFD Simulation for a Turbocharged Heavy Duty Diesel Engine, SAE Technical paper 2011-01-2222, 2011.
22. A. Algieri, M. Amelio, P. Morrone, S. Bova, Energy efficiency analysis of monolith and pellet emission control systems in unidirectional and reverse flow designs, SAE International Journal of Engines, 2 (2010), 684-693.
23. A. Velghe, N. Gillet, J. Bohbot, A high efficiency parallel unstructured solver dedicated to internal combustion engine simulation, Computers & Fluids, 45 (2011), 116-121.
24. A. F. Najafi, S. M. Mousavian, K. Amini, Numerical investigations on swirl intensity decay rate for turbulent swirling flow in a fixed pipe, International Journal of Mechanical Sciences, 53 (2011), 801-811.
25. P. Morrone, A. Algieri, Numerical investigation on the energetic performances of conventional and pellet aftertreatment systems in flow-through and reverse-flow designs, Thermal Science, 15 (2011), 1049-1064.

26. W. Jeong, J. Seong, Comparison of effects on technical variances of computational fluid dynamics (CFD) software based on finite element and finite volume methods, International Journal of Mechanical Sciences, 78 (2014), 19-26.
27. Y. Varol, H.F. Oztop, M. Firat, A. Koca, CFD modeling of heat transfer and fluid flow inside a pent-roof type combustion chamber using dynamic model, International Communication in Heat and Mass Transfer, 37 (2010), 1366-1375.
28. Y. Cai, Z. Liu, Q. Song, Z. Shi, Y. Wan, Fluid mechanics of internal flow with friction and cutting strategies for micronozzles, International Journal of Mechanical Sciences, 100 (2015), 41-49.
29. M. Jia, M. Xie, T. Wang, Z. Peng, The effect of injection timing and intake valve close timing on performance and emissions of diesel PCCI engine with a full engine cycle CFD simulation, Applied Energy 88 (2011) 2967-2975.
30. Y. Yoshihara, K. Nakata, D. Takahashi, T. Omura, A. Ota, Development of high tumble intake-port for high thermal efficiency engines, SAE Technical paper 2016-01-0692, 2016.
31. A. Castilla, M. Rubio, C. Ferrara, J. M. Montanero, J. Fernández, Theoretical and experimental analysis of the steady flow across the cylinderhead of a low-capacity engine, Journal of Applied Mechanics, 83 (2016), in press.
32. C. De Bartolo, A. Algieri, S. Bova, Simulation and experimental validation of the flow field at the entrance and within the filter housing of a production spark-ignition engine, Simulation Modelling Practice and Theory, 41 (2014), 73-86.
33. G. P. Blair, D. McBurney, P. McDonald, P. McKernan, R. Fleck, Some Fundamental Aspects of the Discharge Coefficients of cylinder Porting and ducting Restrictions, SAE Technical paper 980764, 1998.
34. K. E. Bevan, J. B. Ghandhi, PIV Measurements of In-Cylinder Flow in a Four-Stroke Utility Engine and Correlation with Steady Flow Results, SAE Technical paper 2004-32-0005, 2004.

35. J. Rabault, J. A. Vernet, B. Lindgren, P. H. Alfredsson, A study using PIV of the intake flow in a diesel engine cylinder, International Journal of Heat and Fluid Flow, 62 (2016), 56-67.
36. F. Hartmann, S. Buhl, F. Gleiss, P. Barth, M. Schild, S. A. Kaiser, C. Hasse, Spatially resolved experimental and numerical investigation of the flow through the intake port of an internal combustion engine, Oil & Gas Science and Technology, 71 (2016), 1-15.
37. V. R. Pajković, S. V. Petrović, Spatial flow velocity distribution around an inlet port/valve annulus, Thermal Science, 12 (2008), 73-83.
38. L. A. Smith, T. Fickenscher, R. P. Osborne, Engine Breathing – Steady speed volumetric efficiency and its validity under transient engine operation, SAE paper 1999-01-0212, 1999.
39. M. Weclas, A. Melling, F. Durst, Flow Separation in the inlet valve gap of piston engines, Progress in Energy and Combustion Science, 24 (1998), 165-195.
40. J. M. Desantes, J. Benajes, J. Urchueguia, Evaluation of the non-steady flow produced by intake ports of direct injection diesel engines, Experiments in Fluids, 19 (1995), 51-60.
41. SolidWorks Flow Simulation, Technical Reference, 2013.
42. E. A. Fadlun, R. Verzicco, P. Orlandi, J. Mohd-Yosuf, Combined immersed-boundary finite-difference methods for three-dimensional complex flow simulations, Journal of Computational Physiscs, 161 (2000), 35-60.
43. G. Iaccarino, R. Verzicco, Immersed boundary technique for turbulent flow simulations, Applied Mechanics Review, 56 (2003), 331-347.
44. A. Algieri, An Experimental Analysis of the Fluid Dynamic Efficiency of a Production Spark-Ignition Engine during the Intake and Exhaust Phase, ISRN Mechanical Engineering, 2011 (2011), 1-8.
45. A. R. Ismail, R. A. Bakar, Semin, Valve Flow Discharge Coefficient Investigation for Intake and Exhaust Port of Four Stroke Diesel Engines, Journal of Engineering and Applied Sciences, 2 (2007), 1807-1811.

46. G. P. Blair, F. M. M. Drouin, Relationship Between Discharge Coefficients and Accuracy of Engine Simulation, SAE Technical paper 962527, 1996.
47. A. Algieri, S. Bova, C. De Bartolo, Influence of Valve-Lift and Throttle Angle on the Intake Process in High Performance Motorcycle Engine, Journal of Engineering for Gas Turbine and Power, 128 (2006), 934-941.
48. A. Algieri, S. Bova, C. De Bartolo, A. Nigro Numerical and Experimental Analysis of the Intake Flow in a High Performance Four-Stroke Motorcycle Engine, Journal of Engineering for Gas Turbines and Power, 129 (2007), 1095-1105.
49. J. B. Heywood, Internal Combustion Engine Fundamentals, McGraw Hill, New York, 1998.
50. H. Xu, Some Critical Technical Issues on the Steady Flow Testing of Cylinder Heads, SAE Technical paper 2001-01-13, 2001.
51. E. O. Doebelin, Measurement System Application and Design, McGraw Hill, New York, 1990.
52. A. Algieri, S. Bova, C. De Bartolo, Experimental and Numerical Investigation on the Effects of the Seeding Properties on LDA Measurements, Journal of Fluids Engineering, 127 (2005), 514-522.
53. C. S. Peskin, Flow patterns around heart valves: a numerical method, Journal of Computational Physics, 10 (1972), 252-271.
54. J. Mohd-Yusof, Combined immersed boundaries/B-splines methods for simulations of flows in complex geometries, Technical Report, NASA Ames/Stanford University, CTR Annual Research Briefs, 1997.
55. R. Mittal, G. Iaccarino, Immersed boundary methods, Annual Review of Fluid Mechanics 37 (2005) 239-261.
56. C. K. G. Lam, K. Bremhorst, A modified form of the k-ε model for predicting wall turbulence, Journal of Fluids Engineering, 103 (1981), 456-460.

57. W. P. Jones, B. E. Launder, The prediction of laminarization with a two-equation model of turbulence, International Journal of Heat and Mass Transfer, 15 (1972), 301-314.

58. A. Sobachkin, G. Dumnov, Numerical basis of CAD-embedded CFD. In Proceedings of the NAFEMS World Congress, Salzburg (Austria), 2013.

59. B. P. Leonard, A stable and accurate convective modeling procedure based on quadratic upstream interpolation, Computer Methods in Applied Mechanics and Engineering, 19 (1979), 58-98.

60. A. Harten, High resolution schemes for hyperbolic conservation laws, Journal of Computational Physics, 49 (1983), 357-393.

61. A. Harten, On a class of high resolution total variation stable finite difference schemes, Journal on Numerical Analysis, 21 (1984), 1-23.

62. Y. Saad, Iterative methods for sparse linear systems, PWS Publishing Company, Boston 1996.

63. W. Hackbusch, Multi-grid Methods and Applications, Springer-Verlag, NY, 1985.

64. J.-W. Son, S. Lee, B. Han, W. Kim, A Correlation Between Re-Defined Design Parameters and Flow Coefficients of SI Engine Intake Ports, SAE Technical Paper 2004-01-0998, 2004.

65. L. Thobois, G. Rymer, T. Souleres, T. Poinsot, Large-Eddy Simulation IC Engines Geometries, SAE Technical Paper 2004-01-1854, 2004.

66. A. K. Gupta, D. G. Lilley, N. Syred, Swirl Flows, Abacus Press, 1984.

Symbols

A	Area	[m^2]
B	Bore	[m]
C_f	Flow coefficient	[-]

D	Diameter	[m]
Δp	Ambient-cylinder pressure drop	[Pa]
Δp_t	Pressure drop at the throttle valve	[Pa]
F	Throttle angle	[°]
γ	Specific heat ratio	[-]
L	Stroke	[m]
L_v	Valve lift	[m]
$L_{v,j}$	Lift of the generic intake valve j	[m]
$\dot{m}$	Mass flow rate	[kg/s]
N_C	Number of cylinders	[-]
N_v	Number of intake valves per cylinder	[-]
p	Pressure	[Pa]
R	Specific gas constant	[J/kg K]
r	Radial distance	[m]
r_c	Compression ratio	[-]
S	Swirl number	[-]
u	Velocity	[m/s]
z	Distance of the plane from the engine head	[m]

Subscripts

ax	Axial
C	Cylinder
i	Intake
meas	Measured
r	Reference
t	Throttle
tg	Tangential
v	Valve
0	Intake system

Acronyms

AV	Asymmetric Valves lifts
bmep	Brake mean effective pressure
CFD	Computational Fluid Dynamics
DV	Valve Deactivation
IB	Immersed Boundary
ICE	Internal Combustion Engines
SV	Symmetric Valves lifts
TVD	Total Variation Diminishing

List of Figures

Figure 1: Steady flow rig.

Figure 2: 3D CAD model of the engine. Front (a) and lateral (b) views.

Figure 3: Reference planes for the CFD analysis in the cylinder.

Figure 4: Computational domain discretisation. Section of the mesh near the intake valve (a). Three-dimensional hexahedral grid of the cylinder (b).

Figure 5: Influence of valve lift and throttle angle on the engine head flow coefficients for the SV configuration.

Figure 6: Influence of valve lift and throttle angle on the engine flow coefficients for the deactivated DV (a) and asymmetric AV (b) configuration.

Figure 7: Comparison of numerical and experimental flow coefficients for standard (a) and alternative (b) intake strategies.

Figure 8: Pressure-coloured flow trajectories through the engine for SV-F30 (a) and SV-F90 (b) configurations.

Figure 9: Velocity-coloured flow trajectories inside the cylinder. Deactivated valve DV-F90 (a) and symmetric valves SV-F30 (b) configurations.

Figure 10: Velocity-coloured streamtrace distributions on T1 (a,b), T2 (c,d) and T3 (e,f) planes for deactivated valve (DV-F90) and symmetric valves (SV-F30) configurations. Dotted line in DV configuration represents the intake valve that is closed.

Figure 11: Velocity contours on L1 (a,b), L2 (c,d) and L3 (e,f) planes for the deactivated valve (DV-F90) and the symmetric valves (SV-F30) configurations.

Figure 12: Velocity-coloured flow trajectories inside the cylinder for asymmetric valves AV-F90 (a) and symmetric valves SV-F90 (b) configurations.

Figure 13: Velocity-coloured streamtrace distributions on T1 (a,b), T2 (c,d) and T3 (e,f) planes for asymmetric valves (AV-F90) and symmetric valves (SV-F90) configurations.

Figure 14: Velocity contours on L1 (a,b), L2 (c,d) and L3 (e,f) planes for asymmetric valve (AV-F90) and symmetric valves (SV-F90) configurations.

Figure 15: Absolute value of the swirl number on the three transversal planes (T1, T2 and T3) for different valves configurations.

List of Tables

Table 1: Main engine characteristics.

Table 2: Investigated engine configurations and measuring conditions.

Table 3: Analysed configurations with CFD.

Table 4: Grid resolution and computational resources.

Table 5: Boundary conditions.

Table 6: Swirl number on the three transversal planes for different valves configurations.